Crowdsourced Jammer Localization Using APBMs: Performance Analysis Considering Observations Disruption

Andrea Nardin
Politecnico di Torino
Dept. of Electronics & Telecommunications
Turin, Italy
andrea.nardin@polito.it

Tales Imbiriba
Northeastern University
Dept. of Electrical & Computer Eng.
Boston, MA (USA)
talesim@northeastern.edu

Pau Closas
Northeastern University
Dept. of Electrical & Computer Eng.
Boston, MA (USA)
closas@northeastern.edu

Abstract—**Global navigation satellite systems (GNSSs) are a vital technology for many applications. The received signals, however, are weak and easily vulnerable to intentional/unintentional interference. Jamming signals are becoming a serious threat for GNSS users and the localization of the jammer is an effective countermeasure to such attacks. Congested areas are particularly sensitive to these kinds of attacks, but they also present an opportunity to leverage crowdsourced data for threat monitoring purposes. In this context, we foresee a system where agents navigate an area with the ability to transmit the measured signal power, information that can be leveraged for jamming localization purposes. We propose a crowdsourced-based scheme for jammer localization, based on a signal propagation model, enhanced through the use of physics-based path loss modeling and an augmented, data-driven, component. This method can outperform the maximum likelihood estimator in a realistic scenario, despite the limited knowledge of the propagation model. The disruptive effect on agents' own position estimation affects the final jammer localization outcome, which is evaluated in this paper. In the work, we provide extensive experimentation to measure the effect of denied or degraded positioning on crowdsourced estimation as a function of relevant parameters such as agents' positioning error, observation density, and measurement noise.**

Index Terms—**Jamming localization, GNSS, augmented physics-based model, neural networks.**

I. INTRODUCTION

The monitoring of interference to radionavigation systems is extremely important as it is necessary to ensure the reliable operation of various critical applications that rely on Global Navigation Satellite Systems (GNSSs) and their positioning, navigation and timing (PNT) services. GNSS is a term that refers to various satellite-based navigation systems, such as GPS, Galileo, GLONASS, and Beidou [1], [2]. These systems use a network of satellites that transmit synchronized signals, which allow receivers to calculate their position, velocity, and time (PVT). GNSSs are a vital technology for PNT applications such as intelligent transportation systems and ranging [3]–[7], critical infrastructures [8], [9], environmental [10] and space applications [11], [12], among others. However,

due to the increasing reliance on GNSSs [13], there is a growing concern about their vulnerabilities [14], particularly with regards to the susceptibility of GNSSs to jamming interference [15], [16] and spoofing attacks [17]. Moreover, GNSS signals are very weak and it is quite easy to get access to an effective intentional interference source. Indeed GNSS signals are below a receiver's noise floor because of their spread-spectrum modulation. Therefore, in-band signals with power levels higher than the noise floor could indicate the presence of a jamming signal in the surroundings. It is thus fundamental to develop interference monitoring systems that can detect and locate potential threats in a given area [18], [19].

Congested areas are particularly sensitive to these kinds of attacks, but they also present an opportunity to leverage crowdsourced data to implement such monitoring systems [20]. I.e. even though malicious attackers are more prone to operate, in such areas, there is also a potential abundance of jamming detection events. Moreover, highly-frequented spots are also more likely to have a higher concentration of static internet of things (IoT) devices or 5G nodes, which might integrate GNSS receivers and are presumably aware of their fixed location [21]. Nonetheless, crowdsourcing approaches are becoming particularly relevant as GNSS receivers integration in "smart" devices covers an enormous portion of the receivers' market share [13]. Not surprisingly, many researchers proposed crowdsourcing approaches to tackle jamming localization [22]–[26]. In this context, we foresee a system where agents make observations within an area, have the capabilities of communicating the measured signal power in the GNSS frequency bands, and are aware of their position with some level of accuracy. If a sufficient number of agents collect and transmit this information to a central unit, the data can be used to determine the location of the interference source and take corrective action.

To perform such an inference, however, one needs an accurate signal propagation model. Previous works leveraging crowdsourced data for jamming localization generally assumed a known channel model [23], [25], [26], while others, like in

[22], foresee unknown channels but only within the boundaries of an ideal path loss model's parameters. However, the nominal path loss model is not adequate to model complex—and often crowded—environments like urban or indoor scenarios, due, for example, to reflections and obstructions. It may instead be necessary to use a data-driven method such as a neural network (NN) to augment the path loss model. This enhanced model, called an augmented physics-based model (APBM), can learn those propagation components that cannot be easily modeled through analytical or empirical formulations and rather are strictly dependent on the complex propagation environment [27], [28]. Different implementations of APBMs have been successfully used in different contexts [29]–[31].

The use of APBMs to tackle the jammer localization problem was recently introduced in [27], [28] in a baseline scenario, considering static agents, with exact knowledge of their position. However, for plain GNSS-equipped agents, a jamming event can easily degrade localization capabilities and often completely deny users localization, even over a large area, as shown in a preliminary analysis reported in this work. The ultimate impact depends on many factors such as the presence of obstructions to the jamming signal, the jammer transmitting power and signal characteristics, and the agent equipment and conditions. In particular, a GNSS receiver might be enhanced with anti-jamming solutions, able to provide a position fix even in close proximity to the jammer [32]. Moreover, many agents (e.g. smartphones) can rely on alternative location-dependent measurements (inertial navigation systems (INSs), cellular networks), and are able to propagate their position with a degraded accuracy, even under severe jamming [22]. Other static agents might serve also as network nodes (e.g. IoT devices or 5G nodes) and their position knowledge is unaffected by the interference. Nonetheless, agents' reliability might be partially known at a system level and can be leveraged to improve the estimation process. Overall, the jamming impact heavily depends on the crowdsourcing scenario in its entirety, mainly causing (*i*) a reduction of available observations and (*ii*) a degraded agents position estimation, in a variable mixture.

This motivates the analysis reported in this work, where the jammer localization performance is tested against both agents' position estimation accuracy and density of jamming power observations. These parametric analyses allow to thoroughly characterize the proposed APBM technique, without focusing on a specific scenario, whose outcome would largely depend on arbitrary assumptions about the jammer and the crowdsourced devices. We complement the analysis with an investigation of the effect of measurement noise on the jammer position estimation, both with accurate and uncertain agents' positions. Two representative jamming signal propagation scenarios are addressed to assess the proposed method. An open-sky scenario in which the log-distance path loss is an accurate model [33]; and a more complex urban scenario, in which the measured power levels of the received signals are generated using ray tracing techniques [34], [35] and the APBM can show its superiority to plain path loss modeling.

The rest of the paper is organized as follows. Section II presents the localization of a jammer and discusses the use of a nominal path loss propagation model. The section also derives the Cramér-Rao bound (CRB) and maximum likelihood estimator (MLE) for estimation accuracy under the nominal model. Section III introduces the APBM. Section IV provides experimental results to quantify the impact of a jammer on agents' position estimation capabilities. Then, the robustness of the jammer localization method is assessed against different levels of agents' position accuracy and observation density under both path loss and urban propagation scenarios. The final section summarizes the main conclusions and future prospects of the work.

II. PATHLOSS-BASED ESTIMATION OF JAMMER'S POSITION

A. The path loss measurement model

In the proposed framework, the position of the jammer is estimated from a sequence of N observations of the jammer power at different agents' locations. Each observation is related to the vector of parameters to be estimated by a general model, that can be expressed as

$$y_n = f(\mathbf{x}_n; \boldsymbol{\theta}) + \xi_n \tag{1}$$

where y_n is the n-th observation in dBW. The generic function $f(\mathbf{x}_n; \boldsymbol{\theta})$ depends on $\mathbf{x}_n = (x_n^{(1)}, \ldots, x_n^{(D)})^\top$, the location of the agent, and is parametrized by $\boldsymbol{\theta} = (\theta_1, \ldots, \theta_D)^\top$, the jammer's coordinates in D dimensions (usually $D = 3$). In (1), ξ_n is the additive measurement noise, which is assumed to be independent of $\mathbf{x}_n$ and $\boldsymbol{\theta}$. Such a measurement model is particularly useful in the context of GNSS interference because the signals are received below the noise floor, hence large signal powers can be considered as indications of jamming.

The log-distance *path loss* model is a widely adopted model for received signal strength (RSS) observations [36] and can be used to explicitly define $f(\mathbf{x}_n; \boldsymbol{\theta})$ such that

$$f(\mathbf{x}_n; \boldsymbol{\theta}) = P_0 - \gamma 10 \log_{10} d(\mathbf{x}_n, \boldsymbol{\theta}) . \tag{2}$$

In (2), P_0 is the jammer power in dBW at the reference distance of $1\,\text{m}$, and $d(\mathbf{x}_n, \boldsymbol{\theta})$ is the distance between the n-th observer at $\mathbf{x}_n$ and the jammer [33]. It is defined as

$$d(\mathbf{x}_n, \boldsymbol{\theta}) = \|\mathbf{x}_n - \boldsymbol{\theta}\| = \sqrt{(\mathbf{x}_n - \boldsymbol{\theta})^\top (\mathbf{x}_n - \boldsymbol{\theta})} \tag{3}$$

with $\| \cdot \|$ being the Euclidean norm.

Agents locations are generally known to some precision. Without loss of generality, we model such error on the estimated position $\hat{\mathbf{x}}_n = (\hat{x}_n^{(1)}, \ldots, \hat{x}_n^{(D)})^\top$, such that

$$\hat{x}_n^{(i)} \sim \mathcal{N}(x_n^{(i)}, \sigma_{\text{pos}}^2), \quad i = 1, \ldots, D . \tag{4}$$

B. The Cramér-Rao bound

The CRB sets the lower theoretical limit achievable by an unbiased estimator $\hat{\boldsymbol{\theta}}$ of the parameters $\boldsymbol{\theta}$ in terms of its variance. As a result

$$\text{var}([\hat{\boldsymbol{\theta}}]_i) \geq [\boldsymbol{I}^{-1}(\boldsymbol{\theta})]_{ii} \tag{5}$$

where $[\boldsymbol{I}(\boldsymbol{\theta})]_{ij}$ is an element of the Fisher information matrix (FIM).

When the adopted model is the one in (2), the noise term ξ_n in (1) models the unpredictable shadowing effects experienced by measurements. It has been shown in [37], [38] that in nominal conditions this term can be modeled with a log-normal distribution [37], [38], hence resulting in

$$\xi_n \sim \mathcal{N}(0, \sigma^2) \qquad (6)$$

when values are expressed in dB as in (2).

This allows computing the FIM for the general Gaussian case [39], which under the assumption of independent measurements and constant variance can be simplified to

$$[\boldsymbol{I}(\boldsymbol{\theta})]_{ij} = \frac{1}{\sigma^2} \sum_{n=1}^{N} \frac{\partial f(\mathbf{x}_n; \boldsymbol{\theta})}{\partial \theta_i} \frac{\partial f(\mathbf{x}_n; \boldsymbol{\theta})}{\partial \theta_j} \ . \qquad (7)$$

Particularizing this expression for our case using (2), we get

$$\boldsymbol{I}(\boldsymbol{\theta}) = \frac{100\gamma^2}{\sigma^2(\ln(10))^2} \sum_{n=1}^{N} \frac{1}{d^4(\mathbf{x}_n, \boldsymbol{\theta})} (\boldsymbol{\theta} - \mathbf{x}_n)(\boldsymbol{\theta} - \mathbf{x}_n)^{\top} \ . \qquad (8)$$

By replacing (8) into (5), the CRB for the i-th element of $\hat{\boldsymbol{\theta}}$ can be obtained. When $D = 2$, the inverse of $\boldsymbol{I}(\boldsymbol{\theta})$ can be easily computed leading to

$$\mathrm{var}(\hat{\theta}_1) \geq \frac{\sigma^2(\ln(10))^2}{100\gamma^2} \frac{b}{ab - c^2} \qquad (9)$$

$$\mathrm{var}(\hat{\theta}_2) \geq \frac{\sigma^2(\ln(10))^2}{100\gamma^2} \frac{a}{ab - c^2} \ . \qquad (10)$$

where we defined

$$a = \sum_{n=1}^{N} \frac{(\theta_1 - x_n^{(1)})^2}{d^4(\mathbf{x}_n, \boldsymbol{\theta})} \qquad (11)$$

$$b = \sum_{n=1}^{N} \frac{(\theta_2 - x_n^{(2)})^2}{d^4(\mathbf{x}_n, \boldsymbol{\theta})} \qquad (12)$$

$$c = \sum_{n=1}^{N} \frac{(\theta_1 - x_n^{(1)})(\theta_2 - x_n^{(2)})}{d^4(\mathbf{x}_n, \boldsymbol{\theta})} \ . \qquad (13)$$

The interested reader can refer to our previous work [27], [28] for a complete derivation.

C. Maximum Likelihood Estimator

To provide a theoretical benchmarking solution to our analysis, we compute the MLE for a generic measurement model such as the one defined in (1). For this, let us define a dataset $\mathcal{D} = \{y_n, \mathbf{x}_n\}_{n=1}^{N}$ composed of N i.i.d. pairs of RSS measurements y_n and *loci* $\mathbf{x}_n$. Then, because of (1) and (6), the log-likelihood function is

$$\ln p(\mathbf{y}|\mathbf{X}, \boldsymbol{\theta}) = -\frac{N}{2} \ln(2\pi\sigma^2) - \frac{1}{2\sigma^2} \sum_{n=1}^{N} (y_n - f(\mathbf{x}_n; \boldsymbol{\theta}))^2 \qquad (14)$$

where $p(\mathbf{y}|\mathbf{X}, \boldsymbol{\theta})$ is the likelihood function of the observed data $\mathbf{y} = (y_1, \dots, y_N)^{\top}$ and $\mathbf{X} = \{\mathbf{x}_1, \dots, \mathbf{x}_N\}$. The MLE

for the jammer's location, $\hat{\boldsymbol{\theta}}$, can be found by maximizing the log-likelihood as

$$\hat{\boldsymbol{\theta}}_{\mathrm{MLE}} = \arg \max_{\boldsymbol{\theta}} \ln p(\mathbf{y}|\mathbf{X}, \boldsymbol{\theta}) \ . \qquad (15)$$

The widely adopted log-distance path loss model does not hold for small values of distance. Indeed, $f(\mathbf{x}_n; \boldsymbol{\theta}) \to \infty$ when $d(\mathbf{x}_n, \boldsymbol{\theta}) \to 0$, causing the presence of singularities in the likelihood function. These special cases need to be addressed to support the computation of (15) through optimization methods. To this purpose, we modified (2) to

$$\bar{f}(\mathbf{x}_n; \boldsymbol{\theta}) = P_0 - \gamma 10 \log_{10}\{\max(d(\mathbf{x}_n, \boldsymbol{\theta}), d_F)\} \ . \qquad (16)$$

In the equation, d_F is the far-field distance. It is a limit above which the far-field assumption holds, motivating the path loss formulation in (2) [40]. Adopting (16) we obtain a smoother log-likelihood function, fostering its maximization through gradient-based methods [27], [28]. This approach is effectively exploited also to minimize the cost function of the augmented model, as described in the following section.

III. AUGMENTED PHYSICS-BASED ESTIMATION OF JAMMER'S POSITION

The path loss model in equation (2) is effective for describing the RSS in open spaces or as a first approximation, but it does not account for the additional complexities that can occur in urban or indoor environments, where there may be multiple reflections and signal fading. On the other hand, using a NN without incorporating prior information about the propagation laws often requires a large amount of data to accurately model the jamming field. With this in mind, we exploit an augmented approach, where a physics-based model, in this case the modified path loss $\bar{f}(\mathbf{x}_n; \boldsymbol{\theta})$, is expanded by a data-driven component, $g(\mathbf{x}_n; \boldsymbol{\phi})$ which can be implemented through a NN, being $\boldsymbol{\phi} \in \mathbb{R}^M$ the vector of NN's parameters. This component is supposed to act as a correction term around the path loss function, resulting in the enhanced model

$$h(\mathbf{x}_n; \boldsymbol{\theta}, \boldsymbol{\phi}) = \bar{f}(\mathbf{x}_n; \boldsymbol{\theta}) + g(\mathbf{x}_n; \boldsymbol{\phi}) \ . \qquad (17)$$

The measurement model in (1) becomes therefore

$$y_n = h(\mathbf{x}_n; \boldsymbol{\theta}, \boldsymbol{\phi}) + \xi_n \ , \qquad (18)$$

and is used to build a cost function

$$\mathcal{C}(\mathcal{D}, \boldsymbol{\theta}, \boldsymbol{\phi}) = \sum_{n=1}^{N} |y_n - h(\mathbf{x}_n; \boldsymbol{\theta}, \boldsymbol{\phi})|^2 + \beta \|\boldsymbol{\phi}\|_2^2 \qquad (19)$$

whose minimization leads to the APBM estimation through

$$(\hat{\boldsymbol{\theta}}, \hat{\boldsymbol{\phi}}, \hat{P}_0) = \arg \min_{\boldsymbol{\theta}, \boldsymbol{\phi}, P_0} \mathbb{E}_{\hat{p}(\mathcal{D})} \left\{ \mathcal{C}(\mathcal{D}, \boldsymbol{\theta}, \boldsymbol{\phi}) \right\} \ . \qquad (20)$$

An ℓ_2 regularization is used in the cost function (19) to prevent the NN from growing indefinitely in the tentative to model the complex power field. A scalar term, $\beta \in \mathbb{R}_+$, is controlling the regularization, such that when $\beta = 0$ the NN role in the APBM model prevails, while when $\beta \to \infty$ the NN contribution is limited. In (20), the estimation problem is defined with respect

to the jammer location $\boldsymbol{\theta}$ and the NN's parameters $\boldsymbol{\phi}$ as an empirical risk minimization problem; the expectation operator is taken with respect to the empirical data distribution $\hat{p}(\mathcal{D})$. It is worth stressing that this estimator does not need any information about the characteristics of the jammer (i.e. its transmission power). It can, in fact, learn also P_0 as part of the minimization process described by (20).

Our NN implementation is a feed-forward network with 2 hidden layers of 200 and 100 neurons and a hyperbolic tangent activation function. The models are trained trough batch learning for 200 epochs, with a learning rate of 0.4, using the Adam optimizer [41].

IV. RESULTS AND DISCUSSION

In our analysis, we considered two propagation scenarios for the electromagnetic field produced by the jammer. Our goal is to span the wide range of propagation environments that can be experienced. A first, ideal, scenario is entirely described by the path loss formula in (2) and, in the following, referred to as *path loss scenario*. It is specifically defined by the values reported in Table I and a visual description of the field over an area of $1\,\mathrm{km}^2$ is reported in Figure 1a. A second, more challenging, *urban scenario*, is computed through a ray tracing approach [34], [35] in an urban environment. The parameters for the ray tracing simulation are described in Table II and the resulting field is shown in Figure 2a. In our experiments we compared the estimation performance of the proposed APBM with the MLE, and an NN-only estimation, where $h(\mathbf{x}_n; \boldsymbol{\theta}, \boldsymbol{\phi}) = g(\mathbf{x}_n; \boldsymbol{\phi})$, and therefore without any physics-based prior knowledge on the propagation scenario. The estimation results were aggregated over $N_{\mathrm{MC}} = 50$ Monte Carlo simulations to provide a meaningful characterization. Each Monte Carlo realization involves a different set of measurements y_n and measurement data $\hat{\mathbf{x}}_n$, to avoid conditioning the solution with respect to the agents' layout. The CRB is also reported as an indication of how good the performance of the proposed method is. To compare the different approaches we used the root-mean-square error (RMSE), calculated for each dimension of $\boldsymbol{\theta}$ as

$$\mathrm{RMSE}_{\theta_i} = \sqrt{\frac{1}{N_{\mathrm{MC}}} \sum_{n=1}^{N_{\mathrm{MC}}} (\theta_i - \hat{\theta}_{i,n})^2} \ . \tag{21}$$

TABLE I: Path loss scenario simulated parameters.

Parameter	Value
P_0	10 dBW
γ	2

The computed fields allow us to quantify the jammer effect on a user and its capability to self-localize through GNSSs. In the path loss scenario, it can be easily verified that the minimum received power over the area is around $-50\,\mathrm{dBW}$. Assuming a receiver noise density $N_0 = -204\,\mathrm{dBW}$-Hz [44], we can observe a minimum of jammer-to-noise-density power ratio (J/N_0) of 154 dB-Hz, a value that can likely disrupt any
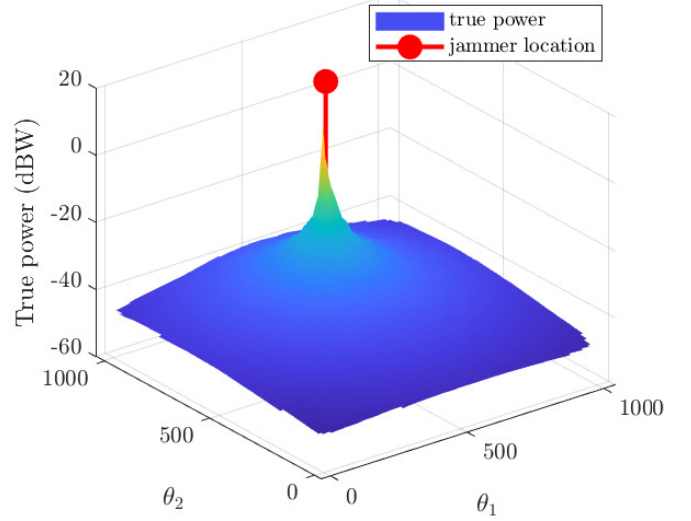
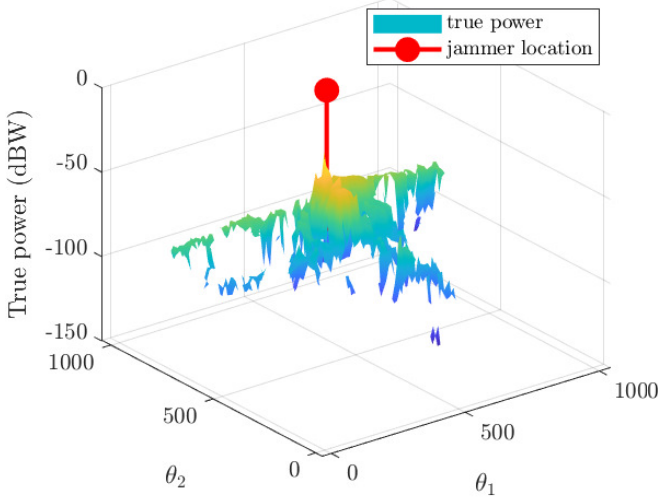(a) Power field over $1\,\mathrm{km}^2$.
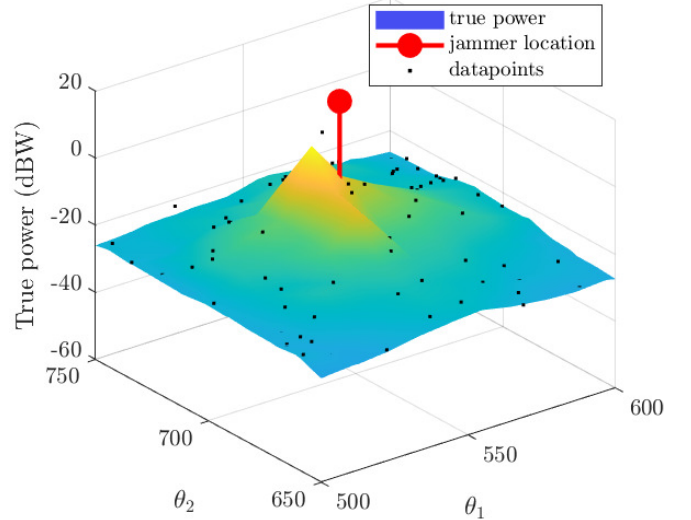
(b) Zoomed-in power field with power observations.

Fig. 1: Jammer power field under path loss conditions.

TABLE II: Raytracing simulation parameters.

Parameter	Value
P_0	10 dBW
Jammer frequency	1575.42 MHz (L1)
Location	41.8800 -87.6295
Max. no. of reflections	4
Ray tracing method	Shooting and bouncing rays (SBR)
Launched rays average separation	0.5391°
Surface material	Concrete [42], [43]
Surface permittivity	$5.31 \cdot \varepsilon_0$ [a]
Surface conductivity	0.0548 S/m

[a] $\varepsilon_0 = 8.8542 \cdot 10^{-12}\,\mathrm{Fm}^{-1}$ is the vacuum dielectric permittivity.

(a) Power field over $1 \, \text{km}^2$.
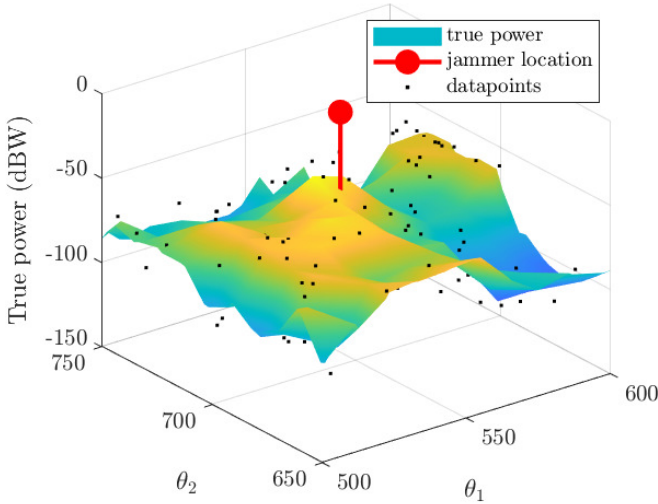
(b) Zoomed-in power field with power observations.

Fig. 2: Jammer power field for a raytracing simulation in urban scenario.

PNT capability of a GNSS receiver over the considered area, especially if no mitigation techniques are implemented [32], [45]. Moving further away from the field peak, the disruptive effect is attenuated. However, because of their weakness and distance from the jammer, observations made at the edges of the observed area are already poorly informative with respect to the jammer's position and this can only get worse as we move away from the power source.

On the other hand, in an urban scenario, the received jamming signal power decreases rapidly due to obstructions and much lower J/N_0 can be experienced within the observed area. In the simulated scenario, for instance, the minimum received power is around $-126 \, \text{dBW}$; a value that, under the

previous assumptions, leads to a J/N_0 of $78 \, \text{dB-Hz}$, a level of interference that can be tolerated by many GNSS receivers in good satellites visibility [32], [45]. Because of the complex propagation scenario, such J/N_0 values are also experienced close to the source (see Figure 2b), however, it is still true that such low values are, on the one hand, poorly informative and, on the other, likely associated with an error-prone agent position estimation because of non-negligible jamming. Both aspects lead to a degraded jammer localization.

A. Impact of estimated agents positions accuracy

Following the previous considerations, the impact of the agents position estimation accuracy on the jammer localization is assessed for different values of σ_{pos}, as defined in (4). A fixed $5 \, \text{dB}$ level of interference-to-noise ratio (INR), defined as

$$\text{INR} = 10 \log_{10} \frac{P_0}{\sigma^2} \tag{22}$$

was chosen to perform the simulation, corresponding to $\sigma = 1.78 \, \text{dBW}$. For this set of experiments, an observation density of $0.01 \, \text{obs./m}^2$ was investigated. This implies one observation every $10 \times 10 \, \text{m}^2$ square, resulting in a total of $10\,000$ power measurements over the observed area of $1 \, \text{km}^2$ for the path loss scenario and 100 measurements over $10\,000 \, \text{m}^2$ for the urban scenario, to limit the computational effort to a practicable amount. Nonetheless, only the 15 largest observations were provided as input to the estimators, which means they were fed with a subset of the datapoints highlighted in Figures 1b and 2b. The resulting RMSEs are reported in Figure 3.

The MLE has a perfect knowledge of the propagation laws experienced by the jamming signal in a path loss scenario. Not surprisingly, focusing on Figure 3a, it can be noticed that the MLE bounds the APBM performance for both components of the estimated parameter. On the other hand, the augmented model performance is very close to the MLE, despite its deficient model, lacking the knowledge of the jammer transmission power. For high σ_{pos}, the MLE starts diverging from the APBM. This may happen because the increased uncertainty on the agents' position tricks the latter into trusting less the path loss model, yielding power to the NN component, which cannot provide an estimate that is as good as the MLE output in this scenario. Indeed, it can be seen in Figure 3a, how the NN-only estimation struggles to accurately model the path loss field.

On the contrary, as shown in Figure 3b, the more complex scenario of Figure 2b cannot be modeled correctly by the MLE, which is mismodeling the field. Nonetheless, also the NN-only estimator is outperformed by the APBM because of its lacking of a priori information about the propagation physics. This means that, although not sufficient by itself, the path loss propagation is a relevant model also in this complex urban scenario, encouraging our adaptive approach. Because of the more challenging propagation environment, it is now harder to provide a correct estimation and a generally higher RMSE can be observed. The agents position error has again
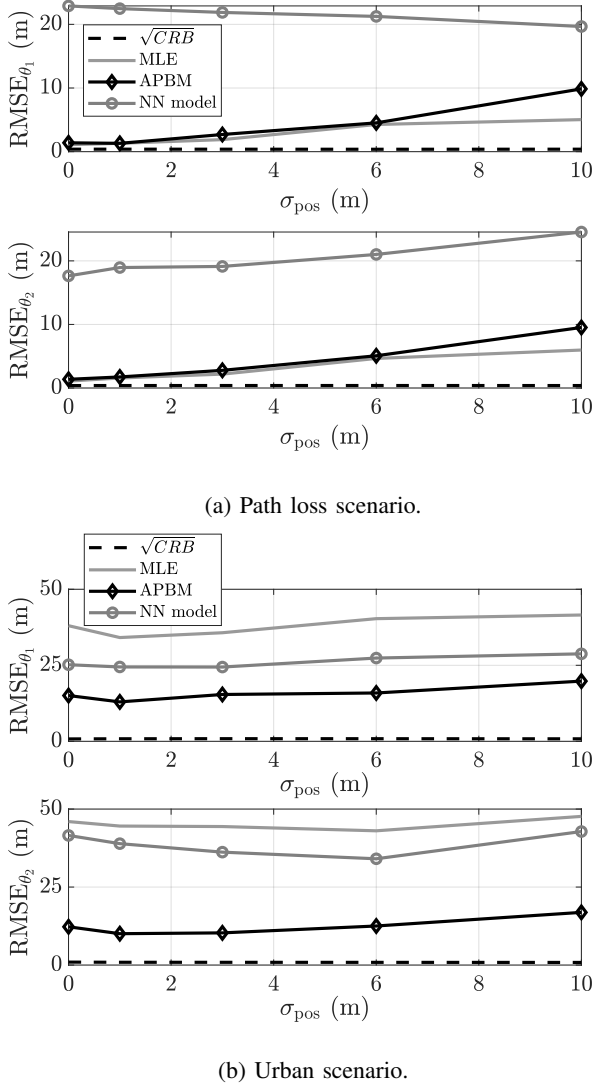
(a) Path loss scenario.

(b) Urban scenario.

Fig. 3: RMSE of jammer position estimation against agents' position accuracy.

a similar impact, moving the final estimation of about $10\,\text{m}$ when σ_{pos} varies from 0 to $10\,\text{m}$.

B. Impact of observation density

As discussed in Section I, some agents may be more resilient than others to the disruptive action of a jammer, causing a plethora of different behaviors. The resulting scenario largely depends on the assumptions made about the devices participating to the crowdsourcing, whose number can be highly reduced under a jamming signal. It is thus important to study the effect, on the proposed estimation method, of a reduced number of observations over an area, as we do in the following by varying the observation density.

The resulting RMSEs are reported in Figure 4 and were obtained with a constant INR of $5\,\text{dB}$ and no uncertainty on

the estimated agents position to avoid conditioning the results with other error sources.

As expected, the RMSE gets better as the observation density increases; this is more evident in the path loss scenario, reported in Figure 4a and particularly in a zoomed-in version, in Figure 4b. Nonetheless, even when moving from 40 to 120 observations over a square of $100 \times 100\,\text{m}^2$, the RMSE variation is limited to few meters. This suggests that, as long as the observations are informative, i.e. they are powerful and not buried into the measurement noise, we need very few measurements to locate the jammer. In an urban scenario, it is more likely to have uninformative measurements, due to obstructions and other signal weakening phenomena. With less, important, observations, reducing the datapoints can result in the loss of measurements that are more relevant than others in the estimation process. Despite the fact that each Monte Carlo realization involves a different agents distribution, because of the fixed environment geometry (e.g. building locations), the estimations of θ_1 and θ_2 are not affected in the same way by the scarcity of measurements. In Figure 4c for instance, when passing from 60 to 40 observations per $100 \times 100\,\text{m}^2$, we have a remarkable performance drop for RMSE_{θ_2}. Potentially, this is because, on average, a value as low as $4 \cdot 10^{-3}\,\text{obs./m}^2$ is enough to dramatically cut down the profitable observations for the estimation of θ_2.

C. Impact of measurement noise

Fixing the observation resolution to $0.01\,\text{obs./m}^2$ and the agents position estimation noise ($\sigma_{\text{pos}} = 10\,\text{m}$), we can observe the combined effect of this error source while varying the INR. The resulting RMSE outcomes are reported in Figure 5.

Also in this analysis, we can see that the MLE can outperform the augmented model only in an ideal propagation environment, such as the path loss scenario investigated in Figure 5a, where the MLE has a perfect knowledge of the model. In a realistic scenario, the MLE cannot reach the performance of the APBM due to mismodeling, as shown in Figure 5b. The NN-only estimator instead, while doing better than the MLE in the urban environment, it is still outperformed by the APBM estimator in both propagation scenarios. Performance gaps aside, it is worth noting that all the estimators cannot improve above a certain INR, reaching a plateau. This means that the achievable performance is limited by the inaccurate position of the agents, which unsurprisingly worsen the final jammer location estimation. Interestingly enough, the minimum RMSE reached in the ideal path loss scenario is around $10\,\text{m}$, which is also the value of σ_{pos} in this experiment (Figure 5a). A relationship that can be verified also by looking at Figure 3a.

This bounding effect of the agents position uncertainty can be easily confirmed by looking at Figure 6, where the previous experiment is repeated using exact agents positions. In the ideal case, the estimators can reach arbitrary good performances, approaching the CRB (Figure 6b). The urban scenario instead challenges the estimation method highlighting its limits, also without errors on agents positions estimations.
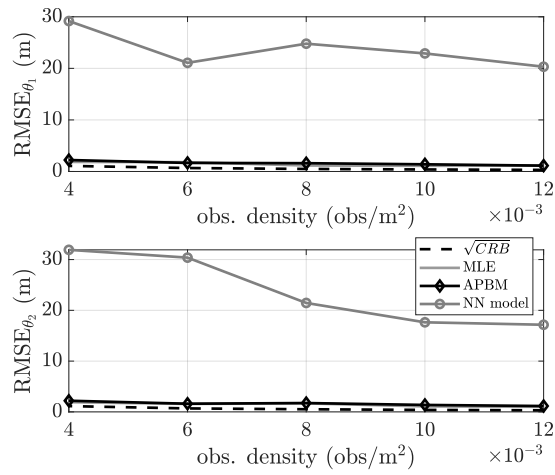
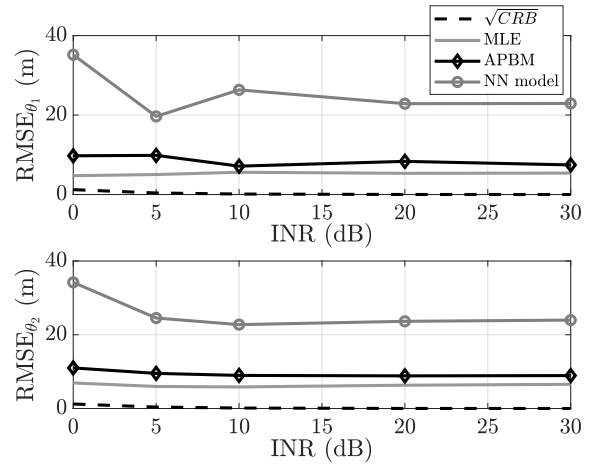(a) Path loss scenario.
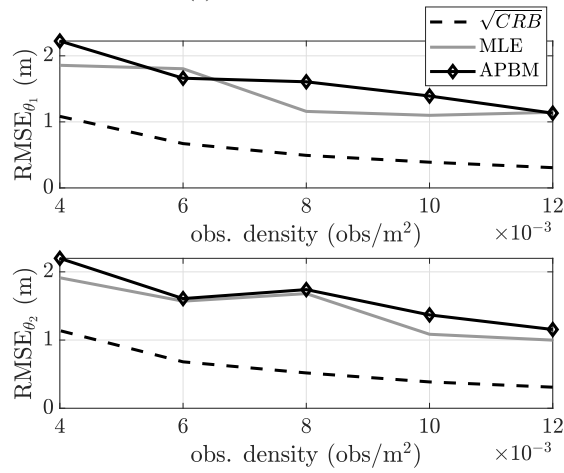
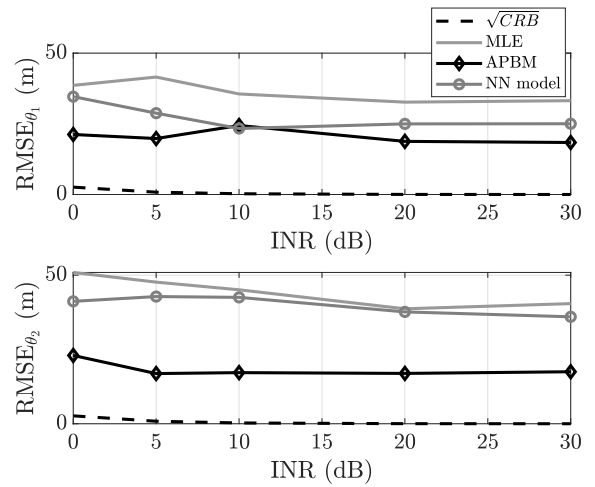(b) Path loss scenario. Zoomed-in.
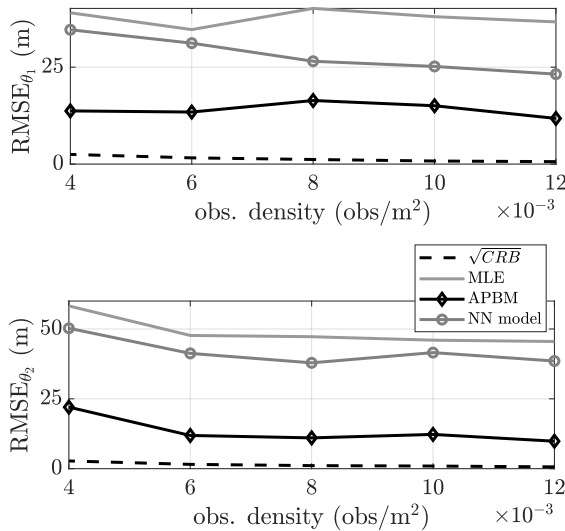
(c) Urban scenario.

Fig. 4: RMSE of jammer position estimation against observation density.
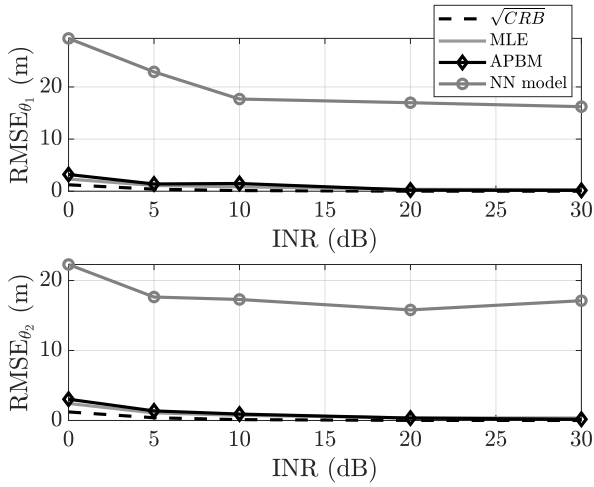

(a) Path loss scenario.

(b) Urban scenario.

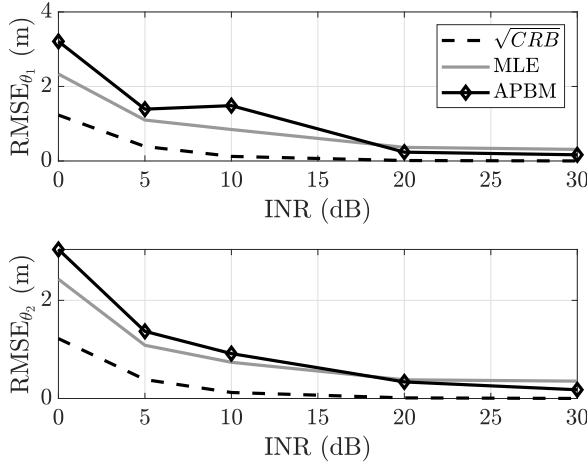Fig. 5: RMSE of jammer position estimation against INR with agents position estimation affected by error.

The resulting RMSE values cannot approach zero due to the complex propagation environment and the lack of very close observations around the main peak. Nevertheless, the APBM outperforms both the MLE and the NN-only estimator even in this complex and unpredictable scenario and without the need to know the jammer transmission power.
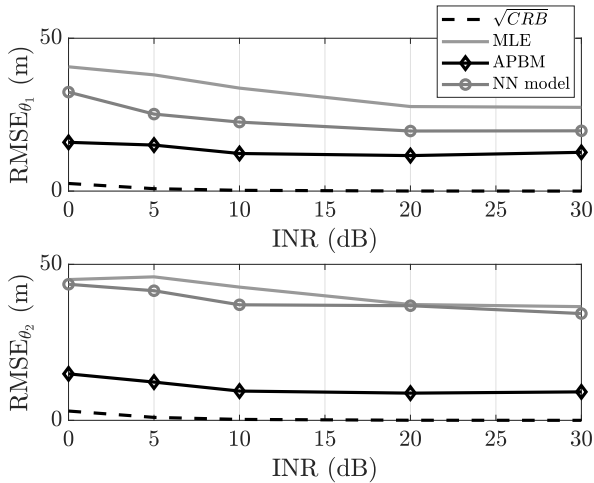
V. CONCLUSION

This paper proposes to leverage crowdsourced data from a number of agents navigating an area, with the purpose of localizing GNSS jamming sources. Compared to other approaches this solution fuses the information from a multitude of receivers, as opposed to having a more specific jamming localization solution based on multi-antenna [46] or synthetic aperture [47] solutions. The proposed localization scheme is based on maximum likelihood estimation, while using an augmented physics-based model (APBM) to better characterize

the propagation channel experienced by the jamming signal in the area of interest. APBMs are a family of powerful data-driven models, which preserve available physics knowledge regarding the problem. The article showed outstanding jammer localization results of APBMs in challenging urban scenarios under a variety of realistic errors and nuisances affecting the capabilities of the collaborative agents. This method proved to seamlessly adapt to very different propagation scenarios, without any prior information about the characteristics of the jammer.

(a) Path loss scenario.

(b) Path loss scenario. Zoomed-in.

(c) Urban scenario.

Fig. 6: RMSE of jammer position estimation against INR without agents position estimation errors.

REFERENCES

[1] D. Dardari, P. Closas, and P. M. Djurić, "Indoor tracking: Theory, methods, and technologies," *IEEE Transactions on Vehicular Technology*, vol. 64, no. 4, pp. 1263–1278, Apr. 2015.

[2] Y. J. Morton, F. van Diggelen, J. J. Spilker Jr, B. W. Parkinson, S. Lo, and G. Gao, *Position, navigation, and timing technologies in the 21st century: integrated satellite navigation, sensor systems, and civil applications*. John Wiley & Sons, 2021.

[3] A. Yastrebova, M. Höyhtyä, S. Boumard, E. S. Lohan, and A. Ometov, "Positioning in the arctic region: State-of-the-art and future perspectives," *IEEE Access*, vol. 9, pp. 53 964–53 978, 2021.

[4] N. Williams, P. B. Darian, G. Wu, P. Closas, and M. Barth, "Impact of Positioning Uncertainty on Connected and Automated Vehicle Applications," *SAE International Journal of Connected and Automated Vehicles*, vol. 6, no. 12-06-02-0010, 2022.

[5] A. Minetto, A. Nardin, and F. Dovis, "Tight integration of GNSS measurements and gnss-based collaborative virtual ranging," in *Proceedings of the 31st International Technical Meeting of the Satellite Division of The Institute of Navigation (ION GNSS+ 2018)*, 2018, pp. 2399–2413.

[6] ——, "GNSS-only collaborative positioning among connected vehicles," in *Proceedings of the 1st ACM MobiHoc Workshop on Technologies, MOdels, and Protocols for Cooperative Connected Cars*, ser. TOP-Cars '19. Association for Computing Machinery, 2019, p. 37–42.

[7] ——, "Modelling and experimental assessment of inter-personal distancing based on shared gnss observables," *Sensors*, vol. 21, no. 8, 2021. [Online]. Available: https://www.mdpi.com/1424-8220/21/8/2588

[8] R. T. Ioannides, T. Pany, and G. Gibbons, "Known vulnerabilities of global navigation satellite systems, status, and potential mitigation techniques," *Proceedings of the IEEE*, vol. 104, no. 6, pp. 1174–1194, 2016.

[9] M. Pini, A. Minetto, A. Vesco, D. Berbecaru, L. M. C. Murillo, P. Nemry, I. De Francesca, B. Rat, and K. Callewaert, "Satellite-derived time for enhanced telecom networks synchronization: the root project," in *2021 IEEE 8th International Workshop on Metrology for AeroSpace (MetroAeroSpace)*, 2021, pp. 288–293.

[10] R. Imam, M. Pini, G. Marucco, F. Dominici, and F. Dovis, "Data from GNSS-Based Passive Radar to Support Flood Monitoring Operations," in *2019 International Conference on Localization and GNSS (ICL-GNSS)*, 2019, pp. 1–7.

[11] A. Minetto, F. Dovis, A. Nardin, O. Vouch, G. Impresario, and M. Musmeci, "Analysis of GNSS data at the Moon for the LuGRE project," in *2022 IEEE 9th International Workshop on Metrology for AeroSpace (MetroAeroSpace)*, 2022, pp. 134–139.

[12] A. Nardin, A. Minetto, O. Vouch, M. Maiani, and F. Dovis, "Snapshot acquisition of GNSS signals in space: a case study at lunar distances," in *Proceedings of the 35th International Technical Meeting of the Satellite Division of The Institute of Navigation (ION GNSS+ 2022)*, Denver, Colorado, September 2022, pp. 3603 – 3617.

[13] European Union Agency for the space program, "EUSPA EO and GNSS market report," EUSPA, Tech. Rep., 2022.

[14] M. G. Amin, P. Closas, A. Broumandan, and J. L. Volakis, "Vulnerabilities, threats, and authentication in satellite-based navigation systems [scanning the issue]," *Proceedings of the IEEE*, vol. 104, no. 6, pp. 1169–1173, 2016.

[15] D. Borio, F. Dovis, H. Kuusniemi, and L. L. Presti, "Impact and detection of GNSS jammers on consumer grade satellite navigation receivers," *Proceedings of the IEEE*, vol. 104, no. 6, pp. 1233–1245, 2016.

[16] R. Morales-Ferre, P. Richter, E. Falletti, A. de la Fuente, and E. S. Lohan, "A survey on coping with intentional interference in satellite navigation for manned and unmanned aircraft," *IEEE Communications Surveys Tutorials*, vol. 22, no. 1, pp. 249–291, 2020.

[17] H. Sathaye, G. LaMountain, P. Closas, and A. Ranganathan, "SemperFi: A Spoofer Eliminating GPS Receiver for UAVs," in *Proceedings of Network and Distributed System Security Symposium (NDSS 2022)*, 2023.

[18] F. Dovis, *GNSS interference threats and countermeasures*. Artech House, 2015.

[19] S. Thombre, M. Z. H. Bhuiyan, P. Eliardsson, B. Gabrielsson, M. Pattinson, M. Dumville, D. Fryganiotis, S. Hill, V. Manikundalam, M. Pölöskey *et al.*, "GNSS threat monitoring and reporting: Past, present, and a proposed future," *The Journal of Navigation*, vol. 71, no. 3, pp. 513–529, 2018.

[20] E. Arias-de Reyna, P. Closas, D. Dardari, and P. M. Djuric, "Crowd-based learning of spatial fields for the internet of things: From harvesting of data to inference," *IEEE Signal Processing Magazine*, vol. 35, no. 5, pp. 130–139, 2018.

[21] R. Prieto-Cerdeira, L. Ries, S. Grec, Florin-Catalinand Cioni, R. De Gaudenzi, and M. Manteiga Bautista, "The role of GNSS in 5G wireless networks," in *NAVITEC 2018*, December 2018.

[22] G. K. Olsson, E. Axell, E. G. Larsson, and P. Papadimitratos, "Participatory sensing for localization of a GNSS jammer," in *2022 International Conference on Localization and GNSS (ICL-GNSS)*, 2022, pp. 1–7.

[23] P. Wang and Y. T. Morton, "Efficient weighted centroid technique for crowdsourcing GNSS RFI localization using differential RSS," *IEEE Transactions on Aerospace and Electronic Systems*, vol. 56, no. 3, pp. 2471–2477, 2020.

[24] L. Strizic, D. M. Akos, and S. Lo, "Crowdsourcing GNSS jammer detection and localization," in *Proceedings of the 2018 International Technical Meeting of The Institute of Navigation*, Feb. 2018, pp. 626–641.

[25] R. C. Blay and D. M. Akos, "GNSS RFI localization using a hybrid TDOA/PDOA approach," in *Proceedings of the 2018 International Technical Meeting of The Institute of Navigation*, Feb. 2018, pp. 703–712.

[26] D. Borio, C. Gioia, A. Štern, F. Dimc, and G. Baldini, "Jammer localization: From crowdsourcing to synthetic detection," in *Proceedings of the 29th International Technical Meeting of the Satellite Division of The Institute of Navigation (ION GNSS+ 2016)*, Sep. 2016, pp. 3107–3116.

[27] A. Nardin, T. Imbiriba, and P. Closas, "Jamming source localization using augmented physics-based model," 2022. [Online]. Available: https://arxiv.org/abs/2212.08097

[28] ——, "Jamming source localization using augmented physics-based model," in *ICASSP 2023 - 2023 IEEE International Conference on Acoustics, Speech and Signal Processing (ICASSP)*, 2023, [in press, preprint available: 10.48550/ARXIV.2212.08097].

[29] A. Demirkaya, T. Imbiriba, K. Lockwood, S. Rampersad, E. Alhajjar, G. Guidoboni, Z. Danziger, and D. Erdoğmuş, "Cubature Kalman Filter Based Training of Hybrid Differential Equation Recurrent Neural Network Physiological Dynamic Models," in *2021 43rd Annual International Conference of the IEEE Engineering in Medicine Biology Society (EMBC)*, 2021, pp. 763–766.

[30] H. Li, R. A. Borsoi, T. Imbiriba, P. Closas, J. C. M. Bermudez, and D. Erdoğmuş, "Model-based deep autoencoder networks for nonlinear hyperspectral unmixing," *IEEE Geoscience and Remote Sensing Letters*, vol. 19, pp. 1–5, 2022.

[31] T. Imbiriba, A. Demirkaya, J. Duník, O. Straka, D. Erdogmus, and P. Closas, "Hybrid neural network augmented physics-based models for nonlinear filtering," in *2022 25th International Conference on Information Fusion (FUSION)*, 2022, pp. 1–6.

[32] H. Li, D. Borio, and P. Closas, "Dual-Domain Robust GNSS Interference Mitigation," in *Proceedings of the 32nd International Technical Meeting of the Satellite Division of The Institute of Navigation (ION GNSS+ 2019)*, Sep. 2019, pp. 991–1002, iSSN: 2331-5954.

[33] T. S. Rappaport, *Wireless Communications: Principles and Practice, 2nd Edition*. Upper Saddle River, New Jersey: Prentice Hall, 2002, pp. 102–105.

[34] K. Schaubach, N. Davis, and T. Rappaport, "A ray tracing method for predicting path loss and delay spread in microcellular environments," in *[1992 Proceedings] Vehicular Technology Society 42nd VTS Conference - Frontiers of Technology*, 1992, pp. 932–935 vol.2.

[35] Z. Yun and M. F. Iskander, "Ray tracing for radio propagation modeling: Principles and applications," *IEEE Access*, vol. 3, pp. 1089–1100, 2015.

[36] P. Wu, T. Imbiriba, G. LaMountain, J. Vilà-Valls, and P. Closas, "Wifi fingerprinting and tracking using neural networks," in *Proceedings of the 32nd International Technical Meeting of the Satellite Division of The Institute of Navigation (ION GNSS+ 2019)*, 2019, pp. 2314–2324.

[37] R. Bernhardt, "Macroscopic diversity in frequency reuse radio systems," *IEEE Journal on Selected Areas in Communications*, vol. 5, no. 5, pp. 862–870, 1987.

[38] D. C. Cox, R. R. Murray, and A. W. Norris, "800-MHz attenuation measured in and around suburban houses," *AT & T Bell Laboratories Technical Journal*, vol. 63, no. 6, pp. 921–954, 1984.

[39] S. M. Kay, *Fundementals of Statistical Signal Processing: Estimation Theory*. Upper Saddle River, New Jersey: Prentice Hall, 1993.

[40] T. S. Rappaport, *Wireless Communications: Principles and Practice, 2nd Edition*. Upper Saddle River, New Jersey: Prentice Hall, 2002, pp. 72–73.

[41] D. P. Kingma and J. Ba, "Adam: A method for stochastic optimization," 2014. [Online]. Available: https://arxiv.org/abs/1412.6980

[42] International Telecommunications Union Radiocommunication (ITU-R) Sector, "Effects of building materials and structures on radiowave propagation above about 100mhz," International Telecommunications Union, Recommendation P.2040-2., September 2021. [Online]. Available: https://www.itu.int/rec/R-REC-P.2040-2-202109-I/en

[43] ——, "Electrical characteristics of the surface of the earth," International Telecommunications Union, Recommendation P.527-6., September 2021. [Online]. Available: https://www.itu.int/rec/R-REC-P.527-6-202109-I/en

[44] R. B. Langley, "GPS receiver system noise," *GPS world*, Jun. 1997. [Online]. Available: http://gauss.gge.unb.ca/papers.pdf/gpsworld.june97.pdf

[45] D. Borio, C. O'Driscoll, and J. Fortuny, "GNSS Jammers: Effects and countermeasures," in *2012 6th ESA Workshop on Satellite Navigation Technologies (Navitec 2012) & European Workshop on GNSS Signals and Signal Processing*, Dec. 2012, pp. 1–7, iSSN: 2325-5455.

[46] C. Fernández-Prades, J. Arribas, and P. Closas, "Robust GNSS receivers by array signal processing: Theory and implementation," *Proceedings of the IEEE*, vol. 104, no. 6, pp. 1207–1220, 2016.

[47] G. LaMountain and P. Closas, "Maneuver Optimization for Synthetic Aperture based DOA estimation of GNSS Jammers," in *2020 IEEE/ION Position, Location and Navigation Symposium (PLANS)*. IEEE, 2020, pp. 44–49.